Title: Origin of colossal magneto-resistance in manganites.

Authors: M. Baldini [1*], T. Muramatsu[2], M. Sherafati[3], H-K. Mao[2, 4], L. Malavasi[5], P. Postorino[6], S. Satpathy[3], and V. V. Struzhkin[2].

Affiliations

[1]HPSynC, Carnegie Institution of Washington, Argonne, IL 60439, USA.

[2]Geophysical Laboratory, Carnegie Institution of Washington, Washington, D.C. 20015, USA.

[3]Department of Physics, University of Missouri, Columbia, Missouri 65211, USA.

[4]Center for High Pressure Science and Technology Advanced Research, Shanghai 201203, China.

[5]Department of Chemistry and INSTM, University of Pavia, Viale Taramelli 10-16, Pavia, Italy.

[6]Department of Physics, University of Rome "Sapienza", P.le A. Moro 5 I-00185 Rome, Italy.

(*)Correspondence and requests for materials should be addressed to mbaldini@carnegiescience.edu

Abstract

Colossal magneto-resistance (CMR), the dramatic reduction of resistance applying a magnetic field, is the core phenomenon for developing new electronic and spintronic devices. In rare earth manganites, this effect has only been observed in doped compounds. The presence of phase separated phases in manganites is widely accepted, however the role of these inhomogeneities in the development of the CMR phenomenon still needs to be clarified. We report the realization of CMR in a pure $LaMnO_3$ manganite. We use pressure to generate a mixed phase constituted by insulating and metallic regions. The CMR takes place when the competition between the two phases is at a maximum. Our results demonstrate in a clean way that phase separation is at the origin of CMR.

Main Text:

In hole-doped rare earth manganite compounds, the CMR peaks at a transition from a high temperature *(T)* insulating paramagnetic phase to a low-*T* conducting ferromagnetic phase. The presence Mn^{3+} and Mn^{4+} ions together with the double-exchange (DE) mechanism *(1)* appear to capture the essence of this phenomenon. A plethora of experimental and theoretical investigations have recently suggested that the ground states of manganites are intrinsically inhomogeneous and are characterized by the presence of competing phases *(2-8)*. High pressure (*P*) has a triggering effect for phase separation since either magnetic or structural domains have been observed in compressed manganites *(9-12)*. However, the role of these nano-clusters in the

CMR phenomenon is still far to be completely understood and designing materials that incorporate CMR at room temperature (*RT*) remains a challenge because of the strong interplay among electronic, structural and magnetic interactions.

As an archetypal cooperative Jahn-Teller (JT) system *(13)* and the parent compound of several important mixed-valence CMR manganite families, $LaMnO_3$ (LMO) is at the focus of intense investigations. Up to now, the CMR effect is only been observed in chemically-doped LMO, but not in pure LMO. At room temperature (*RT*), LMO enters a high conductive phase above 32 GPa showing a "*bad metal*" behavior *(14)*. Previous Raman spectroscopy study *(9)* shows the emergence, in compressed LMO, of a phase separated (PS) state consisting of domains of JT-distorted and undistorted MnO_6 octahedra. The simultaneous presence of an inherent phase separation as well as of a metallization process resembles the conditions under which CMR is observed in doped compounds, and suggests the onset of CMR in compressed LMO. To verify this hypothesis we have carried out an extensive study of the transport properties of LMO over a wide *P*-*T* region ($12<P<54$ GPa and $10<T<300$ K) and applied magnetic field *H*, varying from 0 to 8T. Here we report the realization of CMR in a narrow pressure range between 30 and 35 GPa as the sample transforms from an insulator to a metal. The high pressure insulator to metal transition is described by a percolation mechanism within the phase separated state. This result demonstrates that CMR appearance is possible only because of the presence of a phase separated phase at the percolation threshold.

Electrical resistance, *R*, data measured *in-situ* during the warming cycle in quasi-four probe configuration (Fig. S1) are displayed in Fig.1(a) for $H=0$ and $H=8$T. Three regimes can be identified: a typical semiconductor behavior for $P<32$ GPa; a metallic character for $P>46$ GPa; and an intermediate-*P* range, $32<P<46$ GPa, where the metallization process and CMR are observed. This peculiar behavior can be explained by the *P*-tuning of the intra- and inter-domain interactions.

Lattice compression induces the emergence of small ferromagnetic metallic (FM) domains (undistorted octahedra) with randomly oriented magnetization within an AFM insulating matrix (JT-distorted octahedra). For $P<32$ GPa the large *R* values and their temperature dependences ($dR/dT<0$) are consistent with a PS phase where small FM domains are dispersed in an insulating

matrix (Fig. 1(b)) and do not actually contribute to the system conductivity. The high *T* data are well described by the Efros-Shklovskii variable range hopping law ($R=R_0 \exp(T_0/T)^{1/2}$), which is consistent with the presence of intermixed metallic and insulating regions.

In the high-*P* regime, low *R* values and positive *dR/dT* are observed at *RT*, consistently with the formation of more homogeneous phase with large, oriented, and highly connected FM domains (Fig.1(d)). Wide metallic paths are thus available for spin-polarized conduction. The low-*T* data suggest the presence of a Kondo-like magnetic scattering mechanism (*15, 16*) or grain boundary (GB) effects *(17, 18)* and are well described by a Kondo model *(16)* (Fig. S2). The competition between the AFM and FM phases has been confirmed by *ab initio* calculations *(19)* and support previous Raman results *(9)*. The metallization process is associated with the closure of the e_g band gap and with the crossing of the Fermi level by the unoccupied t_{2g} band *(19)*.

The intermediate-*P* region is nevertheless the most intriguing. Here, although LMO still retains a negative derivative of R *dR/dT*<0, the transition toward a high conductivity phase can be clearly identified. *R* is reduced by more than one order of magnitude on increasing *P* from 30 GPa to 32 GPa, and by four orders of magnitude on compressing from 32 GPa to 42 GPa. Moreover, the 0 K extrapolation of the low-*T* conductivity (inset of Fig.1(a)) displays values definitively greater than zero above 35 GPa, indicating the crossover from an insulating to a high conductive phase. The percolation threshold among conductive FM domains can be identified within the 32-35 GPa range. Further details about compressed LMO in the intermediate pressure regime can be found in the Fig. S3

The most important result is nevertheless the strong magneto-resistance $MR = R(H=0) - R(H)/R(H=0)$ response at around 32 GPa where more than one order of magnitude variation of resistance is observed for an 8 T applied magnetic field (Fig.1(a)). In Fig.2 the MR vs *H* is displayed. MR is around 20% at 12 GPa and continuously increases with *P* until it reaches the maximum value, 80%, at 32 GPa. At 35 GPa, MR drops below 40% and transport properties do not show any significant field dependence above 38 GPa, with MR being around 10%.

The appearance of CMR and its *P*-dependence are consistent with the PS scenario discussed above. At low-*P* the charge transport among weakly connected, small FM clusters is further inhibited by the random orientation of their magnetization (Fig.1(b)). Therefore the applied

magnetic field becomes more and more effective as the volume fraction of the FM domains grows with *P* (Fig. 2(a)-(d)). At 32 GPa, LMO is approaching the percolation threshold and the FM domains come into close contact. The conductivity is thus governed by very close or connected FM clusters and the competition between metallic and insulating clusters is at a maximum (Fig.1(c)). In this peculiar configuration, conduction among the metallic domains depends sensitively on the relative spin orientation of adjacent clusters and remarkable MR originates from the field-induced alignment of FM domains (Fig.1(c) and Fig. 2(e)). The effect of magnetic field is finally reduced with increasing *P* above 35 GPa, where the strong interaction among connected FM domains allows the self-alignment of their magnetization (Fig.1(d)), and conductivity shows only a weak field dependence (Fig. 2(f)-(i)).

Further support to this magnetic PS scenario and to the cluster reorientation effect of the applied field is given by the hysteretic cycles detectable at 32 GPa (Fig. 2(e)). The *memory* effect is quite large. The initial *R* value without field is 40% higher than that one re-obtained at *H*=0 T after the application of the magnetic field due to the residual effect of field induced orientation of the domains (see Fig. 2(e)).

The PS scenario is confirmed by standard percolation theory *(21,22)*. Scaling laws for resistance are given by $R \propto (v - v_c)^{-t}$ and $R \propto (v_c - v)^{s}$ for metallic and insulating regions respectively. Here, v is the volume fraction of each phase. The values of volume fractions were estimated solving a model Hamiltonian describing LMO behavior at *RT*:

$$H = \sum_{\langle ij \rangle,\, \alpha\beta} t_{ij}^{\alpha\beta}\ (\hat{c}_{i\alpha}^{\dagger}\hat{c}_{j\beta} + \text{H.c.}) - g\sum_{i}(Q_{i3}\hat{\tau}_z + Q_{i2}\hat{\tau}_x) + \frac{1}{2}K\sum_{i}(Q_{i3}^2 + Q_{i2}^2) + U\sum_{i}\hat{n}_{i1}\hat{n}_{i2}$$

The first term represents the hopping integral and the last three terms incorporate the Jahn-Teller physics of the Mn e_g electrons and the Coulomb interactions (details about the calculation are in ref *(23)*). The effect of pressure is accounted by a volume dependent hopping integral ($t \propto 1/r^7$) and by adding a Madelung term (-A/r) and an ion-ion repulsive term (B/r^{12}) to the Hamiltonian. The Hamiltonian is solved using the Gutzwiller variational method. The calculated total energy shows a double minimum corresponding to the low-*P* JT distorted insulating phase and the high-*P* undistorted metallic phase. The theoretical volume fractions of each phase were used to fit the R data collected at *RT*. Fig. 3 shows an excellent agreement between theoretical

and experimental data. The predicted percolation pressure, $P_c \approx 30$ GPa, results close to the pressure range determined experimentally. The obtained critical exponents $t = 2.1 \pm 0.2$ and $s = 1.2 \pm 0.2$ are consistent with the expected theoretical values for a three dimensional system *(21, 22)*.

The *T*-*P* phase diagram presented in Fig. 4 basically summarizes the present results. A PS phase is found over a wide *P*-*T* region. At low-*P*, LMO remains in an insulating state. The number and the dimensions of the FM domains as well as the interaction among them progressively grow with pressure, driving domain alignment over a large scale until an extended, connected FM phase is finally established at low-*T* and very high-*P*. Here, LMO displays a metallic character ($dR/dT>0$) and weak field dependence. It is important to point out that the presence of a PS phase is essential for CMR. Indeed the MR increases as the volume fraction of FM phase grows with pressure and peaks at the percolation threshold, when applied magnetic field induces a spin-polarized metallic conduction (orange area in Fig.4). The presence of a FM phase by itself cannot explain the observed CMR. Indeed, above the percolation threshold, where the FM phase is dominant, no significant effects are observed applying magnetic field.

This is in agreement with the unified picture, pointing towards a physics of manganites dominated by coexisting competing phases. However, in typical mixed-valence manganite compounds, the CMR peaks at the insulator to metal transition whereas in LMO, remarkably high MR is obtained just below the percolation threshold among FM domains. This suggests a closer analogy to the negative MR observed in artificial film structures *(24)* composed of nano-scale ferromagnetic particles in an insulating nonmagnetic matrix, and thus to giant MR materials. It is worth noticing that a remarkable difference between these artificial structures and the naturally PS manganites, is the volume/surface ratio of the domains which can be larger in the latter. The nature of this PS state in term of morphology and dynamics of the clusters deserves a deeper and careful investigation. In any case, our discovery has a deep impact on the physics of CMR since it demonstrates that the presence of mixed valence Mn ions is not an essential feature of the CMR phenomenon. Lattice compression induces formation of inhomogeneities driving the system toward a PS state. Nano-scale phase separation by itself is thus the only needed driving force for generating CMR in LMO. The achievement of CMR in a pure system is a key discovery providing the fundamental knowledge for producing CMR compounds by design for practical use under ambient conditions.

References and Notes:

1. C. Zener, Interaction between the *d*-shells in the transition metals. II. Ferromagnetic compounds of manganese with perovskite structure. *Phys. Rev.* **82**, 403 (1951).
2. J. Tao, *et al*., Role of structurally and magnetically modified nanoclusters in colossal magnetoresistance. *Proc. Natl. Acad. Sci.* **108,** 20941 (2011).
3. K. Lai, *et al.,* Mesoscopic percolating resistance network in a strained manganite thin film. *Science* **329**, 190 (2010).
4. M. Fäth, *et al.,* Spatially inhomogeneous metal-insulator transition in doped manganites. *Science* **285**, 1540 (1999).
5. C. Şen, G. Alvarez, and E. Dagotto, Competing ferromagnetic and charge-ordered states in models for manganites: the origin of the colossal magnetoresistance effect. *Phys. Rev. Lett.* **98**, 127202 (2007).
6. J. Tao, *et al.*, Direct imaging of nanoscale phase separation in $La_{0.55}Ca_{0.45}MnO_3$: relationship to colossal magnetoresistance. *Phys. Rev. Lett* **103**, 097202 (2009).
7. E. Dagotto, T. Hotta , and A. Moreo, Colossal magnetoresistant materials: the key role of phase separation. *Physics Reports* **344**, 1 (2001).
8. E. Dagotto, Complexity in strongly correlated electronic systems, *Science* **309**, 257 (2005).
9. M. Baldini, V. V. Struzhkin, A. F. Goncharov, P. Postorino, and W.L. Mao, Persistence of Jahn Teller distortion up to the insulator to metal transition in $LaMnO_3$. *Phys. Rev. Lett.* **106**, 066402 (2011).
10. L. Malavasi, *et al.,* High pressure behavior of Ga-doped $LaMnO_3$: a combined x-ray diffraction and Raman spectroscopy study. *J. Mater. Chem.* **20**, 1304 (2010).
11. M. Baldini, *et al.,* Pressure induced tuning of magnetic phase separation in $Nd_{0.53}Sr_{0.47}MnO_3$. *Phys. Rev. B* **86**. 094407 (2012).
12. M. Baldini, D. Di Castro, M. Cestelli-Guidi, J. Garcia, P. Postorino, Phase-separated states in high-pressure $LaMn_{1-x}Ga_xO_3$ manganites. *Phys. Rev. B* **80**, 045123 (2009).
13. J. Goodenough and J. M. Longo, *Magnetic and Other Properties of Oxides and Related Compound*. edited by K.-H. Hellewege and A. M. Hellewege, Landolt-Borstein Tabellen, New Series, Group 3, Vol 4 (Springer-Verlag, Berlin, 1970).
14. I. Loa, *et al*., Pressure-induced quenching of the Jahn-Teller distortion and insulator-to-metal transition in $LaMnO_3$. *Phys. Rev. Lett.* **87**, 125501 (2001).
15. J. Kondo, Theory of dilute magnetic alloys. *Solid State Phys.* **23**, 183 (1968).
16. J. Zhang, *et al.*, Kondo-like transport and its correlation with the spin-glass phase in perovskite manganites. *Phys. Rev. B* **72**, 054410 (2005).
17. A. Gupta, *et al.*, Grain-boundary effects on the magnetoresistance properties of perovskite manganite films. *Phys. Rev. B* 54**,** R15629 (1996).
18. Y. Xu, J. Zhang, G. Cao, C. Jing, and S. Cao, Low-temperature resistivity minimum and weak spin disorder of polycrystalline $La_{2/3}Ca_{1/3}MnO_3$ in a magnetic field. *Phys. Rev. B* **73,** 224410 (2006).
19. J. He, M. X. Chen, X. Q. Chen, and C. Franchini, Pressure effects on Jahn-Teller distortion in perovskites: The roles of local and bulk compressibilities. *Phys. Rev. B* **85**, 195135 (2012).
20. M. Ziese, and C. Srinitiwarawong, Polaronic effects on the resistivity of manganite thin films. *Phys. Rev. B* **58**, 11519 (1998).

21. B. I. Shklovskii, and A. L. Efros, *Electronic Properties of Doped Semiconductors* (Springer, Berlin, 1984).
22. C. W. Nan, *Physics of inhomogeneous inorganic materials. Prog. Mater. Sci.* ***37****, 1-116* (1993).
23. M. Sherafati, M. Baldini, and S. Satpathy, Percolative Insulator-Metal Transition in LaMnO3, in preparation
24. J. Wu, *et al.*, Intergranular giant magnetoresistance in a spontaneously phase separated perovskite oxide. *Phys. Rev. Lett.* **94**, 037201 (2005).
25. L. Malavasi, M. C. Mozzati, P. Ghigna, C. B. Azzoni, G. and Floris, Lattice disorder, electric properties, and magnetic behavior of $La_{1-x}Na_xMnO_{3+\delta}$ manganites. *J. Phys. Chem. B* **107**, 2500 (2003).
26. A. G. Gavriliuk, A. G. Mironovich, and V. V. Struzhkin, Miniature diamond anvil cell for broad range of high pressure measurements. *Rev. Sci. Instrum.* **80**, 043906 (2009).
27. H-k. Mao, J. Xu, and P. M. Bell, Calibration of the ruby pressure gauge to 800 kbar under quasi-hydrostatic conditions., *J. Geophys. Res.* **91**, 4673 (1986).
28. J.-S. Zhou, Y. Uwatoko, K. Matsubayashi, and J. B. Goodenough, Breakdown of magnetic order in Mott insulators with frustrated superexchange interaction. *Phys. Rev. B* **78**, 220402R (2008).
29. J. Guo, *et al*., Observation of antiferromagnetic order collapse in the pressurized insulator LaMnPO. *Scientific Reports* **3**, 2555 (2013).
30. F. Rivadulla, M. A. Lopez-Quintela, and M. A. Rivas, Origin of the glassy magnetic behavior of the phase segregated state of the perovskites. *Phys. Rev. Lett.* **93**, 167206 (2004).
31. S. Kundu, T. K. Nath, Size-induced metallic state in nanoparticles of ferromagnetic insulating $Nd_{0.8}Sr_{0.2}MnO_3$. *J. Phys.: Condens. Matter* **22**, 506002 (2010).

This work was supported as part of Energy Frontier Research in Extreme Environments Center (***EFree)***, an Energy Frontier Research Center funded by the U.S. Department of Energy, Office of Science under Award Number DE-SC0001057. MS and SS would like to acknowledge the support by the Office of Basic Energy Sciences of the U. S. Department of Energy through Grant Number DE-FG02-00ER45818. The data reported in this paper are all presented in Fig.1 and Fig.3.

Fig.1. (a): Temperature dependence of the resistance $Log_{10}(R/\Omega)$ between 12 and 54 GPa. Solid lines are the data collected at 0 T and dashed lines are the data collected at 8 T. Inset: Temperature dependence of electrical conductivity: the dashed lines indicate the 0 K extrapolation. (b)-(d): schematic sketches of the phase separated state over the three different pressure regimes. (b) P<32 GPa: the volume fraction of the FM region is too small and LMO is an insulator. (c) P=32 GPa: LMO is at the percolation threshold and applied magnetic field induces a spin-polarized metallic conduction and CMR. (d): P>32 GPa: the extended, connected FM phase is finally established.

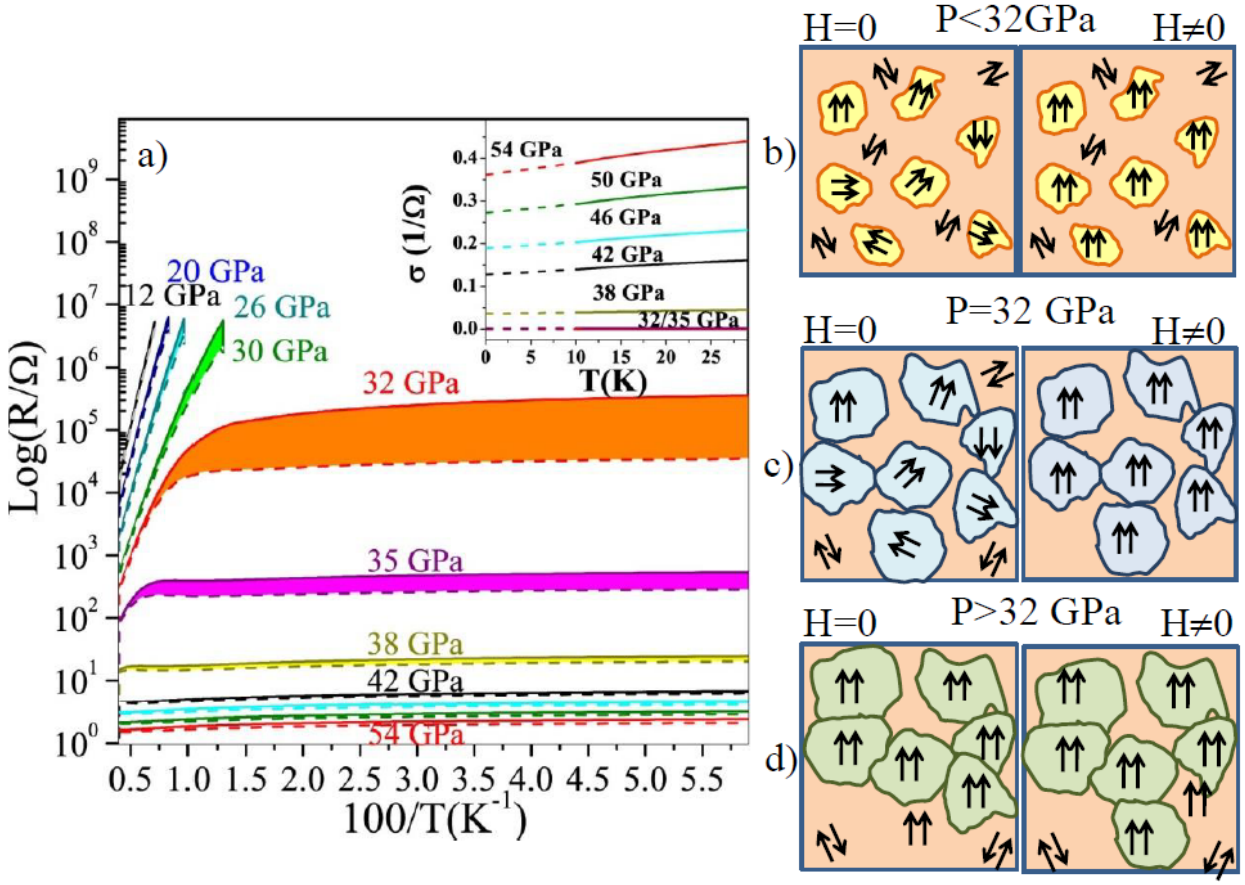

Fig.2. MR percentage as function of pressure. The MR percentage increases from 12 to 32 GPa. At 32 GPa the CMR effect takes place (MR=80%). MR starts to decrease at 35 GPa and it is less than 10 % at 46 GPa. This is consistent with a continuous growth of the volume fraction of the metallic units with pressure. Magnetic field becomes more and more effective as the volume fraction of the metallic clusters increases with pressure (0-30 GPa). CMR is observed at 32 GPa just below the percolation threshold.

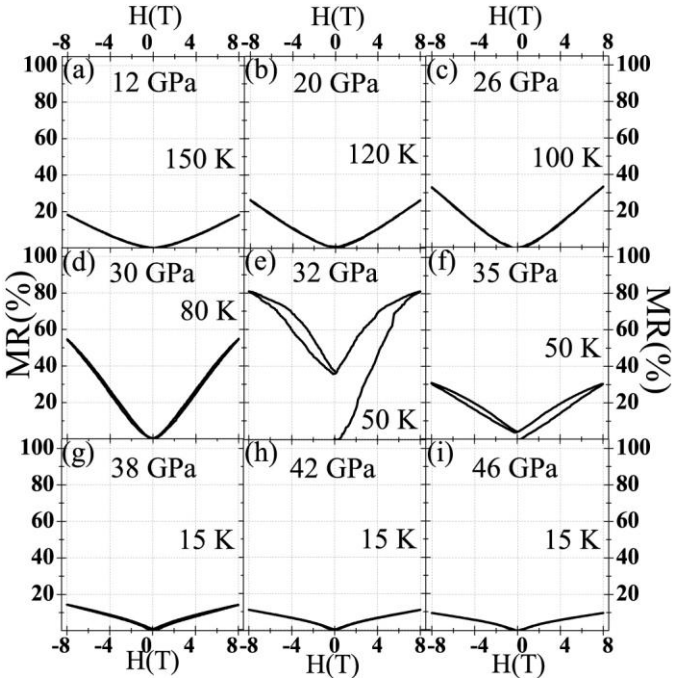

Fig. 3. Natural logarithm of resistance versus pressure at ambient temperature. Red dots represent the experimental resistance data, and the black continuous line is the theoretical curve (best fit parameters v_c*=0.29, t = 2.1± 0.2, s= 1.2±0.2*).

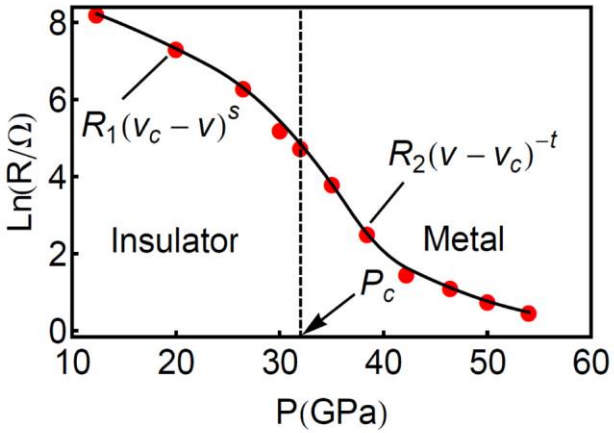

Fig.4. Temperature vs pressure phase diagram of LMO. White diamonds: pressure dependence of T_N *(28)*.. The black and white circles delimit the temperature and pressure regions investigated by Raman spectroscopy[10] and by transport measurements, respectively. The grey line marks the area in which domains are present.

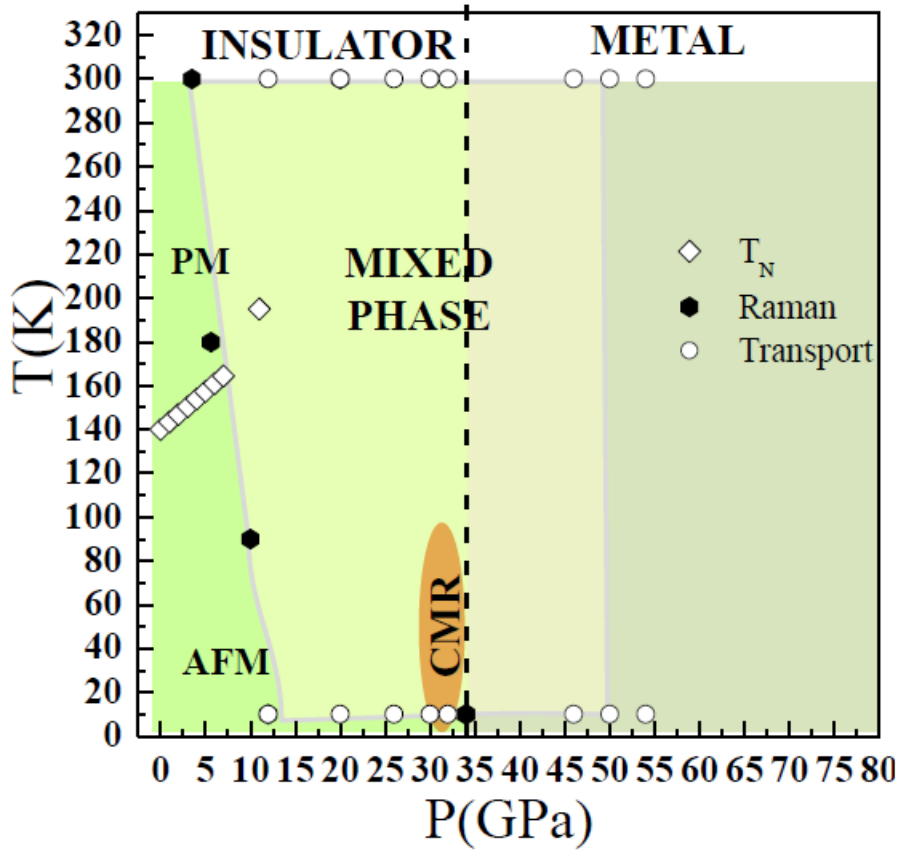

Supplementary Materials:

Materials and methods

Fig.S1-S4

References (24-30)

Materials and Methods:

$LaMnO_3$ sample was synthesized by solid-state reaction starting from proper amounts of La_2O_3 (Aldrich, 99.999%) and Mn_2O_3 (Aldrich, 99.999%). Oxygen stoichiometry was determined by means of thermo-gravimetric analysis *(25)* confirming the correct $LaMnO_3$ stoichiometry.

Magneto-transport experiments were performed using the PPMS facility at Geophysical Laboratory, Carnegie Institution of Washington. A miniature non-magnetic diamond anvil cell was employed *(26).* A Re gasket was initially pre-indented using 300 μm anvils. The bottom part of the gasket chamber was then removed by laser drilling and hexagonal BN was pressed inside the chamber multiple times in order to cover and electrically insulate the edge of the gasket. Black Stycast epoxy was used to insulate the rest of the gasket. LMO powder was then loaded in a 70 micron hole and four platinum leads (2 μm thick) were placed in electric contact with the sample (see extended data Fig. 1). The DAC was electrically connected with PPMS resistivity puck. At each pressure, resistance data were collected over cooling and warming temperature cycles (10-300K) at first without and successively with an 8 T applied magnetic field.

For each pressure point, magneto-resistance MR=R(H=0)-R(H)/R(H=0) data were collected at selected temperatures. MR measurements were taken sweeping the magnetic field in the following way: from *H*=0 T to *H*=8 T, from *H*=8 T to *H*= -8 T and finally from *H*=-8 T to *H*=0 T. A standard symmetric DAC was used as an external press for applying force to PPMS-DAC. Pressure was measured using the ruby fluorescence technique *(27).*

Fig. S1. Photomicrograph of the LMO sample loaded in the PPMS-DAC at 54 GPa. *In-situ* resistance measurements were performed in quasi-four probe configuration using four platinum contacts.

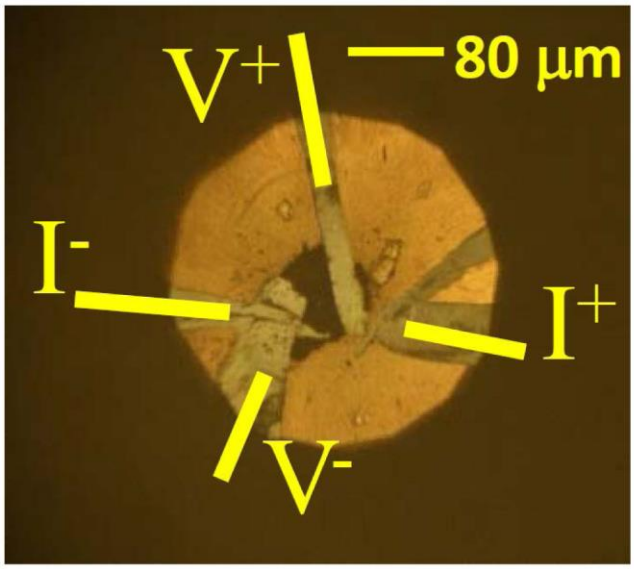

Fig. S2. Resistance data collected between 46 and 54 GPa. The low temperature data are well fitted using a Kondo-like model.

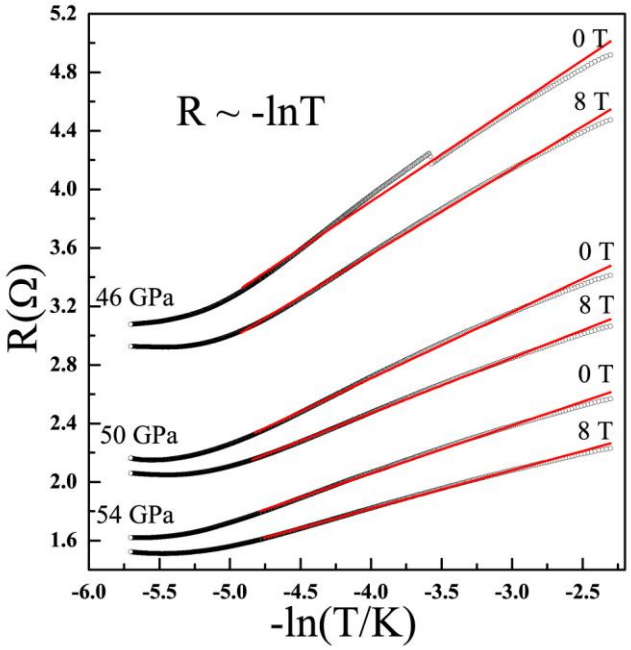

Fig. S3. Temperature dependence of R data at selected pressures during warming temperature cycle. Starting from 32 GPa, a small "bump" (black arrow) is observed in the data collected during the warming cycle. The bump shifts to higher temperatures applying pressure and/or magnetic field and it is suppressed above 42 GPa. At 38 GPa, the sign in the derivative of the resistance becomes positive (*dR/dT>0*) over a narrow temperature range for $T<T_{bump}$. The presence of this bump suggests that itinerant and localized electrons coexist and compete with each other *(29)*. The large residual resistance observed for $T \ll T_{bump}$ can be explained considering magnetic frustration due to inter-cluster interactions *(30)*, and the freezing of the spin clusters *(31)*.

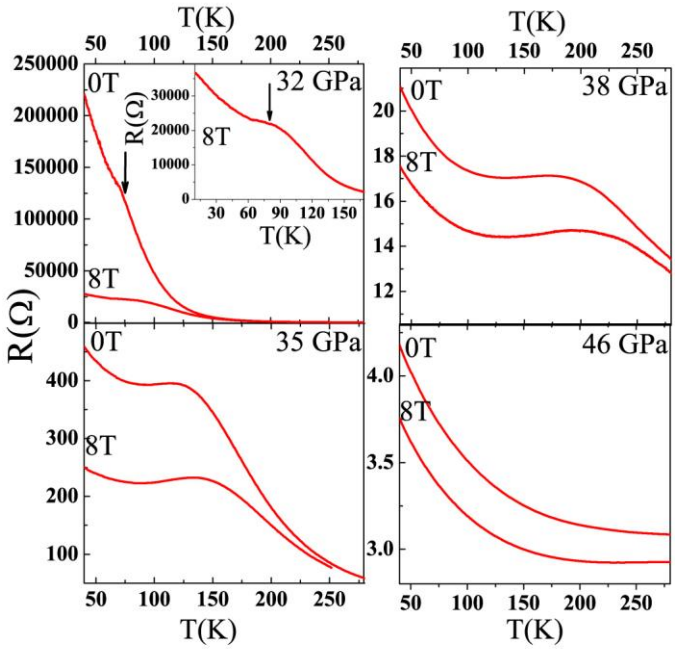
T(K)
R(Ω)
0T
8T
32 GPa
35 GPa
38 GPa
46 GPa